Progress In Electromagnetics Research, Vol. 121, 391–408, 2011

TIME-DOMAIN ITERATIVE PHYSICAL OPTICS METHOD FOR ANALYSIS OF EM SCATTERING FROM THE TARGET HALF BURIED IN ROUGH SURFACE: PEC CASE

J. Li*, B. Wei, Q. He, L. Guo, and D. Ge

School of Science, Xidian University, P. O. Box 274, No. 2 South Taibai Road, Xi'an 710071, P. R. China

Abstract—In this paper, time-domain physical optics (TDPO) method is extended to its iterative version (TDIPO) to consider the coupling effects between two regions, and the latter is employed to investigate electromagnetic scattering from three dimensional target half-buried by a two dimensional rough surface. By using iterative scheme, more accurate transient response reflected from combinative target with multi-scattering effects would be obtained than that by using TDPO alone. The TDIPO could also be enhanced by time-domain equivalent edge current (TDEEC) to further determine the far-field characteristics of the combinative target with rough surface. An accurate composite geometry model technique which combines 2D perfectly electrically conducting (PEC) rough surface and half-buried 3D PEC target is introduced and employed to assist the meshing work. The validity of the presented method is verified by comparing the scattering results for dihedral targets with those obtained through TDPO and finite difference in time domain (FDTD), as well as multi-level fast multiple algorithm (MLFMA). Then simulations of EM scattering from the target embedded in rough surface for different incidence directions are carried out to test the availability of TDIPO/EEC. Discussions on the effects of incidence direction and the presence of the target on the backscattering in far-zone are also given.

1. INTRODUCTION

Nowadays, EM scattering from target above, on, or under rough surface have attracted a lot of researchers' interest, especially three

Received 29 August 2011, Accepted 19 October 2011, Scheduled 2 November 2011

* Corresponding author: Jie Li (li.j1987@gmail.com).

dimensional problems. There are many such applications in real life, which could be called as composite model or combinative model, such as natural or manmade targets on ground and ship over ocean surface. Due to the complex and random nature of rough surface, half-space Green's function method usually fails in such a case, except the approach provided in [1]. Numerical methods such as method of moment (MoM) [2, 3] and finite element method (FEM) [4] are used to study EM scattering from 2D target above 1D rough surface. To improve the efficiency of the these classic approaches, several integral equation-based techniques are proposed, such as multiple sweep method of moments (MSMM) [5], general sparse matrix canonical grid (G-SMCG) [6], fast multipole method (FMM) [7] and generalized forward-backward method (GFBM) [8], as well its extensions, forward-backward method with spectral accelerate algorithm (FBM/SAA) [9] and forward-backward method with extended propagation-inside-layer expansion (FBM/EPILE) [10, 11].

However, the aforementioned numerical methods and their extensions are mainly limited by computer capacity, which restricts their application mostly within 2D case. To overcome the difficulty of modeling the complex interactions of 3D target and 2D rough surface, lots of attempts are made by the EM society, which could be grouped into three categories. The first group includes hybrid methods combining high frequency method with numerical method, such as Kirchhoff approximation-method of moment (KA-MoM) [12] and Kirchhoff approximation multi-level fast multiple algorithm (KA-MLFMA) [13, 14], both of which are proposed using an iterative scheme. The main drawback of this kind of methods is that they are invalid when the target and rough surface touch each other. The second group uses multi-path approach [15], including the application of reciprocity theorem (RT) [16, 17]. These methods simplify the interactions between target and rough surface with first order, second order and high order scattering, leading to a multi-path model, which only requires researchers to consider the effects of most significant scattering-paths. The problem of combinative target-surface, which is the case that this paper mainly handles, cannot be dealt with RT-based multi-path method in [17] because the targets are not detached. The last kind of research is to employ high frequency techniques [18, 19], and this paper mainly contributes to this territory in time domain other than frequency domain in [18, 19]. Time-domain high frequency methods are rarely reported in literatures discussing composite scattering from target above rough surface, although time-domain low frequency methods are reported, such as finite difference in time domain (FDTD) [20–23] and time-domain integral equation

(TDIE) method [24]. Both methods require much computer resource, which limits their usage mostly within 2D and small scale 3D problems.

In this paper, time-domain iterative physical optics (TDIPO) is proposed to consider the multiple scattering effects, which is common in scattering analysis of combinative target and could not modeled easily with time-domain physical optics (TDPO) [25]. The presented TDIPO improves the accuracy of TDPO by employing iteration scheme to get more accurate time-domain currents. The comparison between the transient response of a dihedral structure calculated by TDIPO and that by FDTD and TDPO shows that TDIPO gives acceptable results demonstrating that it is capable of modeling transient response of target with presence of complex interactions between different regions, such as object embedded in rough surface. To consider the diffraction, TDIPO is implemented with an enhancement by using time-domain equivalent edge currents (TDEEC). Also wide-band radar cross section (RCS) is obtained by making Fourier transformation (FT) on time-domain far-field, whose result is verified by comparing with that using sweep-frequency MLFMA. To study wide-band EM scattering of combinative object-rough surface target, an approach building geometry and meshing model of combinative target from generated rough surface is presented. Note that both the rough surface and the target embedded are conducting, and the buried part doesn't need to be meshed in this composite model presented later in this paper. Then TDIPO with TDEEC is applied to the analysis of transient and wide-band scattering of target above or embedded by rough surface, which hasn't been reported in previous literatures, to authors' knowledge.

The remainder of this paper is organized as follows. Section 2 presents the formulation of TDIPO, which is enhanced by TDEEC. Section 3 verifies the validity of TDIPO by comparing the results with those obtained by TDPO, FDTD and MLFMA. Then the next section discusses the procedure of generating composite geometry model and meshing model, which combines two dimensional rough surface and half-buried three dimensional target. Section 5 presents the numerical results. Finally, some concluding remarks are given in the last section.

2. TIME-DOMAIN HIGH FREQUENCY THEORY FOR COMBINATIVE TARGET

High frequency methods such as physical optics (PO), geometrical optics (GO) [26], geometry theory of diffraction (GTD) [27], uniform theory of diffraction (UTD) [28, 29], physical theory of diffraction (PTD) [30], method of equivalent currents (MEC) [31–33] and Equivalent edge currents (EEC) [34] have been applied to scattering

analysis of large target. To model the problem of multiple scattering or coupling between different regions of the object, iterative physical optics (IPO) [35, 36] is employed to study scattering problem such as open-ended cavity.

Besides methods in frequency domain, analysis of wide-band reflected signals directly in time domain [37–42] began to emerge since time-domain physical optics (TDPO) was proposed by Sun [25] in 1994. Most of PO and GO-based high frequency methods in both frequency and time domain have been implemented and used widely, except time-domain version of iterative physical optics which considers multiple scattering directly in time domain. In this section, formulations of TDIPO as well as TDEEC will be given. Note that the following formulations could apply to general model such as scattering from sphere, dihedral and target above rough surface.

2.1. Time-domain Iterative Physical Optics Method

For conducting object, the starting point of time-domain iterative physical optics method is the same as its frequency-domain counterpart, which is magnetic field integral equation (MFIE). On the conductor surface, scattering field can be written as

$$\mathbf{H}_s(\mathbf{r}) = \oint_S \mathbf{J}(\mathbf{r}') \times \nabla' G(\mathbf{r}, \mathbf{r}') ds' \tag{1}$$

where $\mathbf{J}(\mathbf{r}')$ is the electric current induced on the target surface and $G(\mathbf{r}, \mathbf{r}')$ is Green's function in free space. For three dimensional case, $G(\mathbf{r}, \mathbf{r}') = e^{-jk|\mathbf{r}-\mathbf{r}'|}/4\pi|\mathbf{r}-\mathbf{r}'|$. Total field $\mathbf{H}(\mathbf{r}')$ on the surface and $\mathbf{J}(\mathbf{r}')$ could be related using equivalent theorem, which is written as $\mathbf{J}(\mathbf{r}') = \hat{n} \times \mathbf{H}(\mathbf{r}')$, and by interchanging the primed and unprimed coordinates one could also obtain $\mathbf{J}(\mathbf{r}) = \hat{n} \times \mathbf{H}(\mathbf{r})$. Using the assumption that there is no current distribution in regions which could not be illuminated and the Kirchhoff approximation, one can achieve the surface currents referred to as PO currents

$$\mathbf{J}(\mathbf{r}) = \begin{cases} 2\hat{n}(\mathbf{r}) \times \mathbf{H_i}(\mathbf{r}) & \text{lit region} \\ 0 & \text{shadow region} \end{cases} \tag{2}$$

where $\mathbf{H_i}(\mathbf{r})$ denotes the incidence magnetic field.

Instead of directly substituting (2) into (1) to obtain scattering field, which is usually the way for frequency-domain PO solution, one can use an iterative scheme to obtain more accurate currents by considering multiple scattering or coupling effects. In practice, choose the PO currents in (2) as the initial currents $\mathbf{J}_0$ and use the following

equation to get the updated surface currents

$$\begin{aligned}\mathbf{J}_n(\mathbf{r}) &= \mathbf{J}_0(\mathbf{r}) + 2\hat{n} \times \oint_S \mathbf{J}_{n-1}(\mathbf{r}') \times \nabla' G(\mathbf{r}, \mathbf{r}') ds' \\ &= 2\hat{n} \times \mathbf{H}_i(\mathbf{r}) + 2\hat{n} \times \oint_S \mathbf{J}_{n-1}(\mathbf{r}') \times \nabla' G(\mathbf{r}, \mathbf{r}') ds' \end{aligned} \quad (3)$$

where $\mathbf{J}_n$ and $\mathbf{J}_{n-1}$ represent the surface currents of the nth and $(n-1)$th iterations respectively.

Using inverse Fourier transformation (IFT) on (3), one obtains the surface current distribution in time domain. To carry out IFT in a similar way, (3) is rewritten in the following form

$$\begin{aligned}\mathbf{J}_n(\mathbf{r}) &= 2\hat{n} \times \mathbf{H}_i(\mathbf{r}) + 2\hat{n} \times \oint_s \frac{j\omega e^{-jkR}}{4\pi c R^2} \mathbf{J}_{n-1}(\mathbf{r}') \times \mathbf{R} ds' \\ &\quad + 2\hat{n} \times \oint_s \frac{e^{-jkR}}{4\pi R^3} \mathbf{J}_{n-1}(\mathbf{r}') \times \mathbf{R} ds' \end{aligned} \quad (4)$$

where $\mathbf{R} = (\mathbf{r} - \mathbf{r}')$, $R = |\mathbf{R}|$ and c denotes the speed of light in free space. Let $\mathbf{J}_0(\mathbf{r})$, $\mathbf{J}_{n1}(\mathbf{r})$ and $\mathbf{J}_{n2}(\mathbf{r})$ denote the three terms on the right hand of (4), respectively. IFT of these frequency-domain current distributions leads to their corresponding time-domain current distribution, which gives

$$\mathbf{J}_0(\mathbf{r}, t) = 2\hat{n} \times \mathbf{h}_i(\mathbf{r}, t) \quad (5)$$

$$\mathbf{J}_{n1}(\mathbf{r}, t) = 2\hat{n} \times \oint_s \frac{1}{4\pi c R^2} \frac{\partial}{\partial t} \mathbf{J}_{n-1}\left(\mathbf{r}', t - \frac{R}{c}\right) \times \mathbf{R} ds' \quad (6)$$

$$\mathbf{J}_{n2}(\mathbf{r}, t) = 2\hat{n} \times \oint_s \frac{1}{4\pi R^3} \mathbf{J}_{n-1}\left(\mathbf{r}', t - \frac{R}{c}\right) \times \mathbf{R} ds' \quad (7)$$

where $\mathbf{h}_i(\mathbf{r}, t) = \frac{1}{2\pi} \int \mathbf{H}_i(\mathbf{r}, \omega) e^{j\omega t} d\omega$ and $\mathbf{J}_0(\mathbf{r}, t)$ is induced directly by the incident source and called time-domain PO currents. The $t - \frac{R}{c}$ term in (6) and (7) is due to the contribution of other parts of the target and linear property of FT is employed to obtain (6) and (7). By summing up all the current components, one can obtain the time-domain IPO currents distribution in the nth iteration, which is written as follows

$$\mathbf{J}_n(\mathbf{r}, t) = \mathbf{J}_0(\mathbf{r}, t) + \oint_s \left(\frac{1}{c}\frac{\partial}{\partial t} + \frac{1}{R}\right) \frac{2\hat{n}}{4\pi R^2} \times \mathbf{J}_{n-1}\left(\mathbf{r}', t - \frac{R}{c}\right) \times \mathbf{R} ds' \quad (8)$$

The integral term represents the contribution from other regions, which is added upon the original time-domain PO current in non-iterative TDPO formulation. After getting the current distribution in time domain, one could calculate the far-zone scattered field induced by $\mathbf{J}_n(\mathbf{r},t)$ using the following equation

$$\begin{cases} \mathbf{E^s}(\mathbf{r},t) = \frac{Z_0}{4\pi rc}\iint\limits_{s'} \hat{r}\times\left[\hat{r}\times\frac{\partial}{\partial t}\mathbf{J}_n\left(\mathbf{r}',t-\tau_1\right)\right]ds' \\ \mathbf{H^s}(\mathbf{r},t) = -\frac{1}{4\pi rc}\iint\limits_{s'} \hat{r}\times\frac{\partial}{\partial t}\mathbf{J}_n\left(\mathbf{r}',t-\tau_1\right)ds' \end{cases} \tag{9}$$

where Z_0 is the characteristic impedance of free space.

Attention should be paid when one calculates $\mathbf{J}_n(\mathbf{r},t)$ from $\mathbf{J}_{n-1}(\mathbf{r}',t-\tau)$ under the condition of physical optics approximation. Contribution from $\mathbf{J}_{n-1}(\mathbf{r}',t-\tau)$ is only considered when $\mathbf{r}$ and $\mathbf{r}'$ could *see* each other. There's similar case when calculating initiate time-domain current distribution from the incident wave, point source or plane wave source. Certain algorithm should be employed to find the lit region and the shadow region, which has been discussed in previous literatures [37].

2.2. Time-domain Equivalent Edge Current Method

Johansen [43] derived the TDEEC formulation and applied it into the far-field analysis of diffraction of edges of 3D conductors. Altıntas [44] also applied TDEEC to transient scattering analysis. TDEEC is employed to improve the accuracy of TDIPO as its frequency counterpart [34] does to PO. By taking inverse Fourier transformation of the frequency-domain edge currents, one can obtain the equivalent edge currents in time domain. Then time-domain diffracted field can be gotten, which is expressed as [44]

$$\begin{aligned} \mathbf{e}_d^{\mathrm{EEC}}(\mathbf{r},t) = & = \frac{Z_0}{4\pi rc}\hat{s}\times\hat{s}\times\frac{\partial}{\partial t}\oint_c I^f(\mathbf{r}',\tau)\hat{l}dl' \\ & + \frac{1}{4\pi rc}\hat{s}\times\frac{\partial}{\partial t}\oint_c M^f(\mathbf{r}',\tau)\hat{l}dl' \end{aligned} \tag{10}$$

In Equation (10), $\mathbf{e}_d^{\mathrm{EEC}}(\mathbf{r},t)$ is the time-domain diffracted field; $\hat{\mathbf{s}}$ is unit vector in diffraction direction; $\hat{l}dl'$ gives the length element along the edge; the electric edge current $I^f(\mathbf{r}',\tau)$ and magnetic edge current $M^f(\mathbf{r}',\tau)$ are expressed as

$$I^f(\mathbf{r}',\tau) = \int_{-\infty}^{\tau} c\left[Z_0^{-1}D_e^{I,f}\mathbf{e}_i(\mathbf{r}',\tau)\cdot\hat{l} + D_h^{I,f}\mathbf{h}_i(\mathbf{r}',\tau)\cdot\hat{l}\right]dt \tag{11}$$

$$M^f(\mathbf{r}',\tau) = \int_{-\infty}^{\tau} cZ_0D_h^{M,f}\mathbf{h}_i(\mathbf{r}',\tau)\cdot\hat{l}dt \tag{12}$$

where $\mathbf{e}_i$ and $\mathbf{h}_i$ are time-domain incident electric and magnetic fields respectively, and $D_e^{I,f}$, $D_h^{I,f}$ and $D_h^{M,f}$ are diffraction coefficients [44]. For far-field calculation, numerical evaluation of integrals when computing equivalent edge currents is not necessary. Substituting (11) and (12) into (10) gives

$$\mathbf{e}_d^{\mathrm{EEC}}(\mathbf{r},t) = \frac{1}{4\pi r}\hat{s}\times\left[\hat{s}\times\oint_c\left[D_e^{I,f}\mathbf{e}_i(\mathbf{r}',\tau)\cdot\hat{l}+Z_0D_h^{I,f}\mathbf{h}_i(\mathbf{r}',\tau)\cdot\hat{l}\right]\hat{l}dl'\right] + \frac{1}{4\pi r}\hat{s}\times\oint_c Z_0D_h^{M,f}(\mathbf{h}_i(\mathbf{r}',\tau)\cdot\hat{l})\hat{l}dl' \tag{13}$$

For further information on the formulation, one can refer to [44]. By adding the TDEEC term to the transient field obtained by TDIPO, more accurate result could be achieved by considering the curvature effects [43].

3. VALIDATION OF TDIPO/EEC

In this section, TDIPO would be employed to calculate the transient backscattered field of a simple structure to test its accuracy against TDPO and FDTD, as well as MLFMA.

The structure analyzed is a dihedral, which is useful for evaluating a RCS prediction code to consider the contributions of multiple scattering effects between plates. The geometry studied in this section is composed of two square plate with edge length of 0.3 m, with one plate in *yoz* plane and the other in *xoy* plane, and the torsion angle is $\alpha = 90^\circ$. The exciting source is a modulated Gaussian pulse, with frequency band width $f = 4 \sim 6$ GHz and pulse width $\tau = 1.7$ ns. The incidence angle is $\theta_i = 45^\circ$ and azimuths angle is $\phi_i = 0^\circ$. The vector of electric field is along y axis, which is φ polarization.

Figure 1(a) plots the $\varphi\varphi$ polarized backscattered electric field in far-zone computed by TDIPO/EEC, and results achieved by FDTD and TDPO/EEC are also included. The agreement between TDIPO/EEC and FDTD is very good, whereas sharp difference is observed between the curves obtained by TDPO/EEC and FDTD. This is due to the existence of multiple scattering between the two plates, while TDPO/EEC cannot consider the coupling effects, which actually only calculates the single-bounce reflected field, neglecting the two-bounce scattered field. For further verification, Figure 1(b) plots the wide band RCS through carrying out fast Fourier transformation (FFT) on transient response, which is also compared with results by MLFMA with a frequency-sweeping procedure. To measure the agreement of TDIPO/EEC presented in this paper with FDTD or MLFMA in a quantitative way, mean absolute percentage error

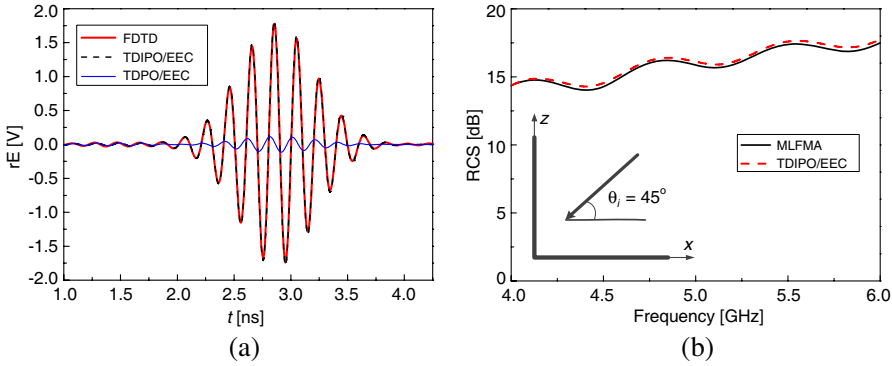

Figure 1. Backscattering of dihedral structure. (a) Transient response. (b) Monostatic RCS.

(MAPE) and mean absolute error (MAE), for time- and frequency-domain study respectively, are employed to evaluate the validation of TDIPO/EEC in modeling scattering from complex structures. In the transient responses scattered by the dihedral plotted in Figure 1(a), MAPE of the time series obtained by TDIPO/EEC is 0.07, while MAPE of TDPO/EEC is as large as 1.04. In the frequency-domain results illustrated in Figure 1(b), MAE of the curve calculated by TDIPO/EEC compared with that of MLFMA is 0.215 dB and the standard deviation is 0.063.

4. COMBINATIVE TARGET MODELING

In this part, combinative target modeling composing 2D rough surface and 3D half-buried target will be presented, which is of great importance for the rough surface scattering analysis in the following section.

The first step is to generate the profile of 2D rough surface, which satisfies the requirements of height distribution function and autocorrelation function, or its frequency counterpart power spectrum density function (FT of autocorrelation function). To obtain the sampling points of rough surface profile, usually a spectral method could be employed. The formula is written as

$$f(x,y) = \frac{1}{L^2} \sum_{m=-N/2}^{N/2-1} \sum_{n=-N/2}^{N/2-1} F(K_{xm}, K_{yn}) \exp(iK_{xm}x + iK_{yn}y) \quad (14)$$

where

$$F(K_{xm}, K_{yn}) = 2\pi L\sqrt{W(K_{xm}, K_{yn})} \begin{cases} [N(0,1) + iN(0,1)]/2 & m, n \neq 0, N/2 \\ N(0,1) & m, n = 0, N/2 \end{cases} \quad (15)$$

K_{xm} and K_{yn} are sampling points of spatial frequency. $W(K_{xm}, K_{yn})$ is power spectrum density function, which could be Gaussian spectrum and ocean wave spectrum, such as Joint North Sea Wave Project (JONSWAP) and Pierson-Moskowitz (PM) spectrum. L is length of the simulated surface. $N(0,1)$ is a random number following some probability density function. If the height distribution function and autocorrelation function are both assumed to be Gaussian type, one calls rough surface of this kind as Gaussian type, which usually could be descripted by root mean square height (σ) and correlation length (l_x, l_y). Figures 2(a)–(d) give several examples of rough surface generated

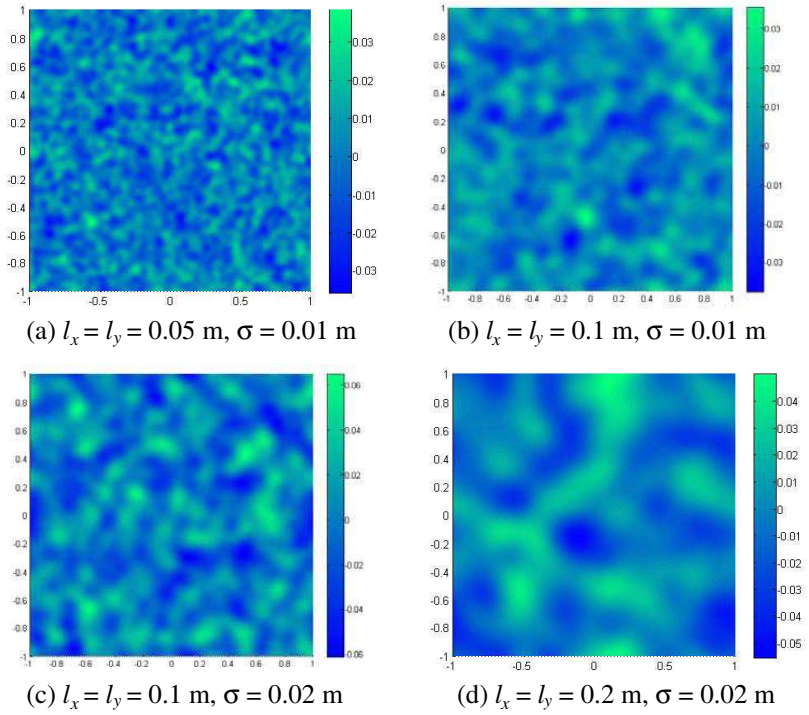

(a) $l_x = l_y = 0.05$ m, $\sigma = 0.01$ m

(b) $l_x = l_y = 0.1$ m, $\sigma = 0.01$ m

(c) $l_x = l_y = 0.1$ m, $\sigma = 0.02$ m

(d) $l_x = l_y = 0.2$ m, $\sigma = 0.02$ m

Figure 2. Examples of simulated random rough surface with certain roughness parameters (the unit of the color bar is meter).

with the parameters below the corresponding plot. The rough surface profiles are all generated using Gaussian type functions, and the choices of parameters are largely random but in the sense of representing typical rough surface with small roughness, like soil surface and even scale model of ocean surface.

After rough surface is generated (sampled), all the sampled points are scattered in the 3D space, called point cloud model [45]. Using an inverse engineering method, rough surface is converted into an NURBS [46] surface. However in the combinative model case, some further work should be done, especially when the buried target is complex in shape. The most important step is to find the intersection curve between 2D rough surface and 3D target accurately, which could be done through Boolean operation [47] of two objects. Finally, a meshing tool is used to get surface meshes with the information of incident wave length. A combinative buried model is built from the randomly generated rough surface in Figure 3(a), and the meshing result of the combinative model is plotted in Figure 3(b).

5. SIMULATION RESULT OF TARGET EMBEDDED IN ROUGH SURFACE

In this section, TDIPO with TDEEC is employed to study the problem of transient scattering, including single rough surface and target on rough surface. Note that in this paper, only rough surface with finite length is considered, so no tapering or window is applied upon the incident pulse, which is a little different from previous research [3, 7]. Geometry of the composite scattering problem could be illustrated as in Figure 4, where some parameters about incidence and polarization are defined.

The first example is to compute the backscattering characteristics

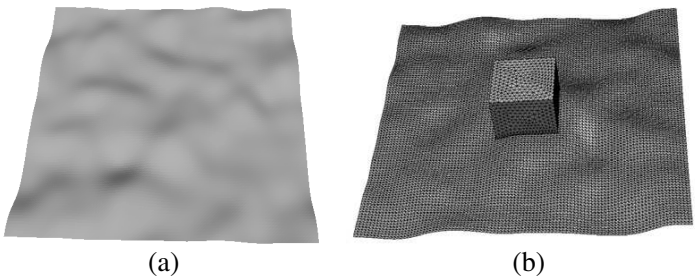

Figure 3. Combinative model. (a) Original rough surface. (b) Meshing.

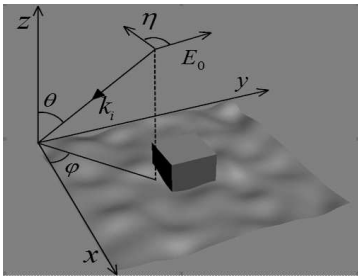

Figure 4. Scattering geometry with relevant parameters definition.

of single rough surface. The size of the rough surface is $1\,\mathrm{m} \times 1\,\mathrm{m}$; root mean square height is $\sigma = 0.01\,\mathrm{m}$; the correlation length is $l_x = l_y = 0.1\,\mathrm{m}$. The incident pulse is the same as the one in the verification section, except incidence angle. The $\varphi\varphi$ polarized backscattered electric fields in time domain are illustrated in Figures 5(a)–(c) for the cases of $\theta_i = 0^\circ$, $\theta_i = 30^\circ$ and $\theta_i = 45^\circ$ respectively, where the azimuth angle is kept as $\varphi_i = 0^\circ$. From these figures, one could find that most of the waveforms obtained by TDIPO/EEC agree well with those by TDPO/EEC. After transforming the transient responses into frequency domain, as illustrated in Figure 5(d), only slight difference in monostatic RCS is observed between the curves obtained by TDIPO/EEC and TDPO/EEC at certain incidence angle. The MAE of the frequency-domain results in Figure 5(d) are 0.00153 dB for $\theta_i = 0^\circ$, and 0.0730 dB for $\theta_i = 30^\circ$ and 1.07 dB for $\theta_i = 45^\circ$, respectively. Therefore in rough surface scattering problem, especially that with small roughness (such as parameters used for generating rough surface examples in Figure 2 at focused frequency band in this paper), TDIPO and TDPO would give similar results with not much disparity, which means TDPO is accurate enough for this case. However, for composite scattering problem like in next example, it is not the same case anymore. Besides, when comparing the results of TDIPO/EEC through Figures 5(a) to 5(c), one can observe that the magnitudes get smaller with increasing incidence angle. This could be understood as that smaller incidence leads to more power scattered into backward direction. And at normal incidence, the backscattering direction coincides with specular direction, which results in very strong transient responses as plotted in Figure 5(a) compared with those in Figures 5(b) and 5(c).

Figures 6(a)–(c) plot the results of $\varphi\varphi$ polarized transient responses from a combinative model combining rough surface and target for different incidence angles. Parameters of underlying rough

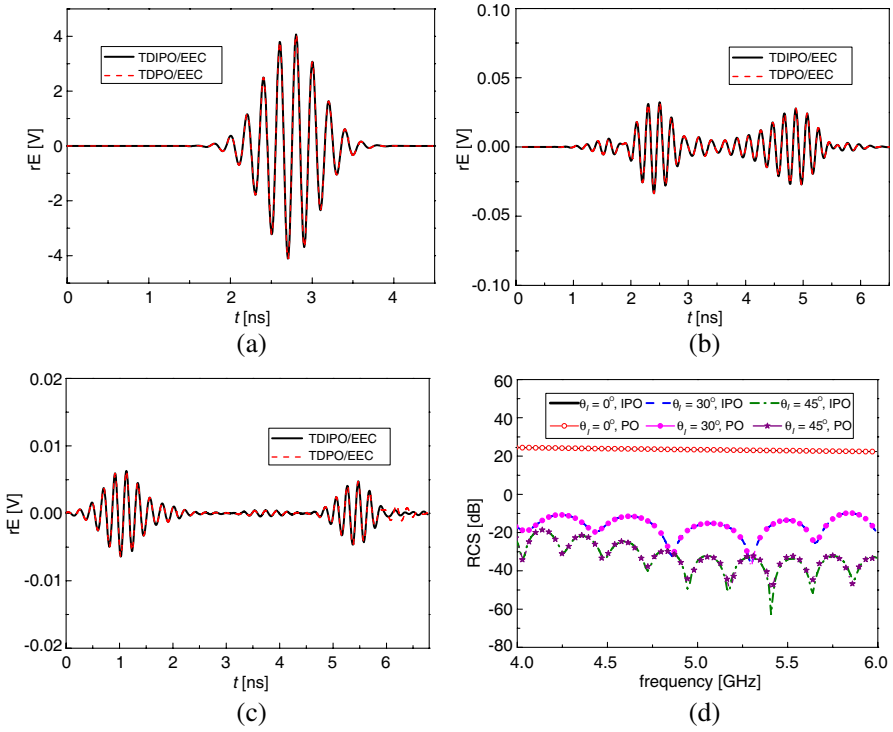

Figure 5. Backscattering of single 2D rough surface. (a) Transient response when $\theta_i = 0°$. (b) Transient response when $\theta_i = 30°$. (c) Transient response when $\theta_i = 45°$. (d) Monostatic RCS (IPO and PO in the legends denote TDIPO/EEC and TDPO/EEC respectively)

surface and the exciting sources are the same as in last simulation. The half-buried target is positioned in the center of the surface, and the above face is square and is 0.2 m × 0.2 m in size and 0.15 m high above the average plane of rough surface, as demonstrated in Figure 3(b). Results calculated by TDIPO/EEC are remarkably different with those by TDPO/EEC, except the normal incidence case given in Figure 6(a). It is found that, in Figures 6(b) and 6(c), the waveforms calculated by TDIPO/EEC give larger values, especially in the middle stage. It is well known that there are interactions between the rough surface and the embedded target surface. The vertical faces of target, together with the underlying rough surface, could be considered as several dihedral structures. From the point view of ray-tracing or GO, at non-normal incidence, dihedral is a typical kind of strong backscattering source due to the double-bounce effect, which could be illustrated

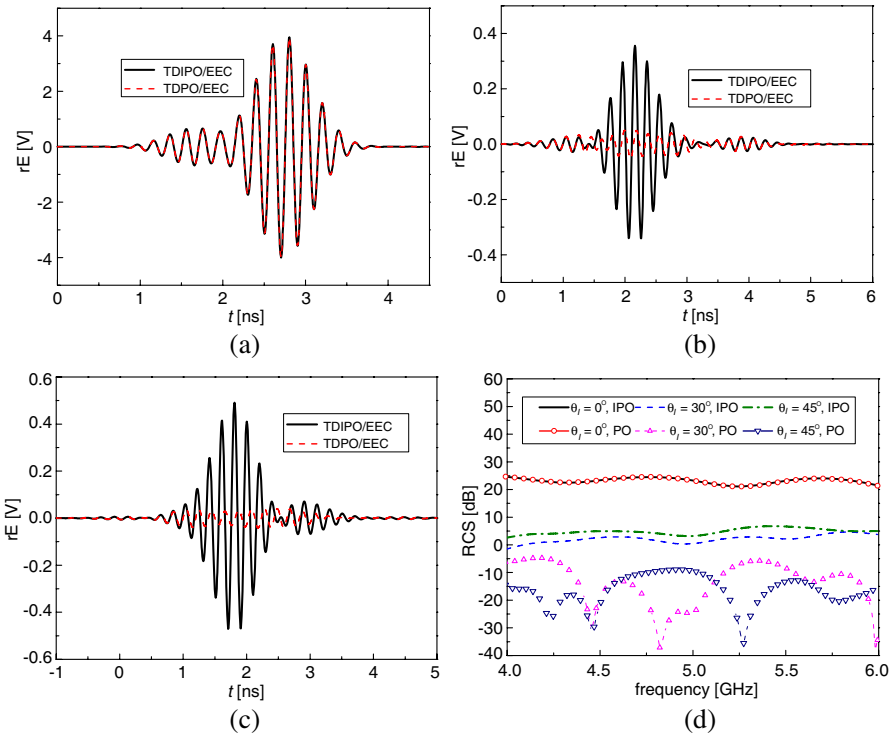

Figure 6. Backscattering of single 2D rough surface and 3D half-buried target. (a) Transient response when $\theta_i = 0°$. (b) Transient response when $\theta_i = 30°$. (c) Transient response when $\theta_i = 45°$. (d) Monostatic RCS.

from the comparison of TDPO/EEC and TDIPO/EEC in Figure 1. Therefore, those interactions will make the backscattered field increase in magnitude, exceeding the availability of TDPO. Moreover, the amplitude for $\theta_i = 45°$ is larger than that for $\theta_i = 30°$, simply because more power is scattered back into the incidence direction for the case of $\theta_i = 45°$. At normal incidence, because *dihedral effect* is very weak, TDPO/EEC could give the results with acceptable accuracy compared with TDIPO/EEC, which is demonstrated in Figure 6(a). The above judgments may be further strengthened by the curves of wide band RCS, as plotted in Figure 6(d). The RCS patterns obtained by TDPO and TDIPO are totally different for $\theta_i = 30°$ and $\theta_i = 45°$, and values of RCS by using TDIPO are larger than those by TDPO at most frequencies. The MAE of the frequency-domain results in Figure 6(d) are 0.0607 dB for $\theta_i = 0°$, and 16.0 dB for $\theta_i = 30°$ and

21.4 dB for $\theta_i = 45°$, respectively. And the RCS curve (obtained by TDIPO/EEC) of $\theta_i = 45°$ is also above the one of $\theta_i = 30°$ through most of the frequency band. Because of presence of strong multi-scattering between rough surface and embedded target, backscattered field would be enhanced as observed in the results of dihedral structure.

6. CONCLUSION

In this paper, a time-domain high frequency TDIPO method is proposed to study transient scattering fields of combinative structure, which also can be used for detached composite model. Through the verification example and other numerical methods, one can find that TDPO is not accurate enough when dealing with complex structure with multiple scattering effects, whereas TDIPO enhanced by TDEEC could give accurate result, showing good agreement with FDTD. Wide-band Radar Cross Section of 3D target on 2D rough surface is also obtained by applying FFT to the obtained time-domain signal, which is of significant use in some practical application, such as target recognition and remote sensing.

ACKNOWLEDGMENT

This work was supported by the National Natural Science Foundation of China (Grant No. 60871071) and by the Fundamental Research Funds for the Central Universities, China. The authors would like to thank the reviewers for their helpful and constructive suggestions.

REFERENCES

1. Guan, B., J. F. Zhang, X. Y. Zhou, and T. J. Cui, "Electromagnetic scattering from objects above a rough surface using the method of moments with half-space Green's function," *IEEE Transactions on Geoscience and Remote Sensing*, Vol. 47, 3399–3405, 2009.
2. Guo, L.-X., A.-Q. Wang, and J. Ma, "Study on EM scattering from 2-D target above 1-D large scale rough surface with low grazing incidence by parallel MoM based on PC clusters," *Progress In Electromagnetics Research*, Vol. 89, 149–166, 2009.
3. Wang, X. and L.-W. Li, "Numerical characterization of bistatic scattering from PEC cylinder partially embedded in a dielectric rough surface interface: Horizontal polarization," *Progress In Electromagnetics Research*, Vol. 91, 35–51, 2009.

4. Liu, P. and Y.-Q. Jin, "An FEM approach with FFT accelerated iterative robin boundary condition for electromagnetic scattering of a target with strong or weak coupled underlying randomly rough surface," *IEEE Transactions on Antennas and Propagation*, Vol. 53, 4137–4144, 2005.
5. Colak, D., R. J. Burkholder, and E. H. Newman, "On the convergence properties of the multiple sweep method of moments," *Applied Computational Electromagnetics Society Journal*, Vol. 22, 207–218, Jul. 2007.
6. Ji, W.-J. and C.-M. Tong, "Bistatic scattering from two-dimensional dielectric ocean rough surface with a PEC object partially embedded by using the G-SMCG method," *Progress In Electromagnetics Research*, Vol. 105, 119–139, 2010.
7. Wang, A. Q., L. X. Guo, and C. Chai, "Fast numerical method for electromagnetic scattering from an object above a large-scale layered rough surface at large incident angle: Vertical polarization," *Applied Optics*, Vol. 50, 500–508, Feb. 2011.
8. Rodriguez Pino, M., L. Landesa, J. L. Rodriguez, F. Obelleiro, and R. J. Burkholder, "The generalized forward-backward method for analyzing the scattering from targets on ocean-like rough surfaces," *IEEE Transactions on Antennas and Propagation*, Vol. 47, 961–969, 1999.
9. Li, Z. and Y.-Q. Jin, "Bistatic scattering and transmitting through a fractal rough surface with high permittivity using the physics-based two-grid method in conjunction with the forward-backward method and spectrum acceleration algorithm," *IEEE Transactions on Antennas and Propagation*, Vol. 50, 1323–1327, 2002.
10. Kubicke, G., C. Bourlier, and J. Saillard, "Scattering by an object above a randomly rough surface from a fast numerical method: Extended PILE method combined with FB-SA," *Waves in Random and Complex Media*, Vol. 18, 495–519, 2008.
11. Bourlier, C., G. Kubické, and N. Déchamps, "Fast method to compute scattering by a buried object under a randomly rough surface: PILE combined with FB-SA," *J. Opt. Soc. Am. A*, Vol. 25, 891–902, 2008.
12. Jin, Y.-Q. and H. Ye, "Bistatic scattering from a 3D target above randomly rough surface," *IEEE International Geoscience and Remote Sensing Symposium*, 57–60, 2007.
13. Zhang, X. Y. and X. Q. Sheng, "Highly efficient hybrid method for monostatic scattering by objects on a rough surface," *IET Microwaves, Antennas & Propagation*, Vol. 4, 1597–1604, 2010.

14. Yang, W., Z. Zhao, C. Qi, W. Liu, and Z.-P. Nie, "Iterative hybrid method for electromagnetic scattering from a 3D object above a 2D random dielectric rough surface," *Progress In Electromagnetics Research*, Vol. 117, 435–448, 2011.
15. Johnson, J. T., "A numerical study of scattering from an object above a rough surface," *IEEE Transactions on Antennas and Propagation*, Vol. 50, 1361–1367, 2002.
16. Dai, S.-Y., C. Zhang, and Z.-S. Wu, "Electromagnetic scattering of objects above ground using MRTD/FDTD hybrid method," *Journal of Electromagnetic Waves and Applications*, Vol. 23, No. 16, 2187–2196, 2009.
17. Wang, Y. H., Y. M. Zhang, M. X. He, and L. X. Guo, "Solution of scattering from rough surface with a 2D target above it by a hybrid method based on the reciprocity theorem and the forward-backward method," *Chinese Physics B*, Vol. 17, 3696–3703, Oct. 2008.
18. Xu, F. and Y.-Q. Jin, "Bidirectional analytic ray tracing for fast computation of composite scattering from electric-large target over a randomly rough surface," *IEEE Transactions on Antennas and Propagation*, Vol. 57, 1495–1505, 2009.
19. Bausssard, A., M. Rochdi, and A. Khenchaf, "PO/MEC-based scattering model for complex objects on a sea surface," *Progress In Electromagnetics Research*, Vol. 111, 229–251, 2011.
20. Li, J., L.-X. Guo, and H. Zeng, "FDTD method investigation on the polarimetric scattering from 2-D rough surface," *Progress In Electromagnetics Research*, Vol. 101, 173–188, 2010.
21. Li, J., L. X. Guo, Y. C. Jiao, and K. Li, "Investigation on wide-band scattering of a 2D target above 1D randomly rough surface by FDTD method," *Optics Express*, Vol. 19, 1091–1100, Jan. 2011.
22. Kuang, L. and Y. Q. Jin, "Bistatic scattering from a three-dimensional object over a randomly rough surface using the FDTD algorithm," *IEEE Transactions on Antennas and Propagation*, Vol. 55, 2302–2312, Aug. 2007.
23. Lee, S.-W., A. Ishimaru, and Y. Kuga, "Numerical analysis of scattered waves from rough surfaces with and without an object," *Surface Scattering and Diffraction for Advanced Metrology II*, 7–14, Seattle, WA, United States, Jul. 9, 2002.
24. Wang, R., L. X. Guo, J. Li, and X. Y. Liu, "Investigation on transient electromagnetic scattering from a randomly rough surface and the perfect electric conductor target with an arbitrary cross section above it," *Science in China Series G — Physics Mechanics & Astronomy*, Vol. 52, 665–675, May 2009.

25. Sun, E.-Y. and W. V. T. Rusch, "Time-domain physical-optics," *IEEE Transactions on Antennas and Propagation*, Vol. 42, 9–15, 1994.
26. Ghaffar, A., A. A. Rizvi, and Q. A. Naqvi, "Fields in the focal space of symmetrical hyperboloidal focusing lens," *Progress In Electromagnetics Research*, Vol. 89, 255–273, 2009.
27. Pelosi, G., R. Tiberio, S. Puccini, and S. Maci, "Applying GTD to calculate the RCS of polygonal plates," *IEEE Transactions on Antennas and Propagation*, Vol. 38, 1294–1298, 1990.
28. Hsu, H.-T., F.-Y. Kuo, and H.-T. Chou, "Convergence study of current sampling profiles for antenna design in the presence of electrically large and complex platforms using fit-UTD hybridization approach," *Progress In Electromagnetics Research*, Vol. 99, 195–209, 2009.
29. Lertwiriyaprapa, T., P. H. Pathak, and J. L. Volakis, "An approximate UTD ray solution for the radiation and scattering by antennas near a junction between two different thin planar material slab on ground plane," *Progress In Electromagnetics Research,* Vol. 102, 227–248, 2010.
30. Ufimtsev, P. Y., "Method of edge waves in the physical theory of diffraction," *Soviet Radio*, Moscow, 1962.
31. Clemmow, P., "Edge currents in diffraction theory," *IEEE Transactions on Antennas and Propagation*, Vol. 4, 282–287, 1956.
32. Ryan, C., Jr. and L. Peters, Jr., "Evaluation of edge-diffracted fields including equivalent currents for the caustic regions," *IEEE Transactions on Antennas and Propagation*, Vol. 17, 292–299, 1969.
33. Wu, Z.-S., J.-J. Zhang, and L. Zhao, "Composite electromagnetic scattering from the plate target above a one-dimensional sea surface: Taking the diffraction into account," *Progress In Electromagnetics Research*, Vol. 92, 317–331, 2009.
34. Michaeli, A., "Equivalent edge currents for arbitrary aspects of observation," *IEEE Transactions on Antennas and Propagation*, Vol. 32, 252–258, 1984.
35. Obelleiro-Basteiro, F., J. L. Rodriguez, and R. J. Burkholder, "Iterative physical optics approach for analyzing the electromagnetic scattering by large open-ended cavities," *IEEE Transactions on Antennas and Propagation*, Vol. 43, 356–361, 1995.
36. Lim, H. and N.-H. Myung, "A novel hybrid AIPO-MoM technique for jet engine modulation analysis," *Progress In Electromagnetics Research*, Vol. 104, 85–97, 2010.

37. Guan, Y., S.-X. Gong, S. Zhang, B. Lu, and T. Hong, "A novel time-domain physical optics for computation of electromagnetic scattering of homogeneous dielectric objects," *Progress In Electromagnetics Research M*, Vol. 14, 123–134, 2010.
38. Qin, S.-T., S.-X. Gong, R. Wang, and L.-X. Guo, "A TDIE/TDPO hybrid method for the analysis of TM transient scattering from two-dimensional combinative conducting cylinders," *Progress In Electromagnetics Research*, Vol. 102, 181–195, 2010.
39. Faghihi, F. and H. Heydari, "A combination of time domain finite element-boundary integral with time domain physical optics for calculation of electromagnetic scattering of 3D structures," *Progress In Electromagnetics Research*, Vol. 79, 463–474, 2008.
40. Faghihi, F. and H. Heydari, "Time domain physical optics for the higher-order FDTD modeling in electromagnetic scattering from 3D complex and combined multiple materials objects," *Progress In Electromagnetics Research*, Vol. 95, 87–102, 2009.
41. Yang, L.-X., D.-B. Ge, and B. Wei, "FDTD/TDPO hybrid approach for analysis of the EM scattering of combinative objects," *Progress In Electromagnetics Research*, Vol. 76, 275–284, 2007.
42. Luo, W., W.-Y. Yin, M.-D. Zhu, and J.-Y Zhao, "Hybrid TDIE-TDPO method for studying on transient responses of some wire and surface structures illuminated by an electromagnetic pulse," *Progress In Electromagnetics Research*, Vol. 116, 203–219, 2011.
43. Johansen, P. M., "Time-domain version of the physical theory of diffraction," *IEEE Transactions on Antennas and Propagation*, Vol. 47, 261–270, 1999.
44. Altintas, A. and P. Russer, "Time-domain equivalent edge currents for transient scattering," *IEEE Transactions on Antennas and Propagation*, Vol. 49, 602–606, 2001.
45. Sitek, A., R. H. Huesman, and G. T. Gullberg, "Tomographic reconstruction using an adaptive tetrahedral mesh defined by a point cloud," *IEEE Transactions on Medical Imaging*, Vol. 25, No. 9, 1172–1179, 2006.
46. Wang, A. Q., L. X. Guo, and C. Chai, "Numerical simulations of electromagnetic scattering from 2D rough surface: Geometric modeling by NURBS surface," *Journal of Electromagnetic Waves and Applications*, Vol. 24, No. 10, 1315–1328, 2010.
47. De Berg, M., O. Cheong, M. van Kreveld, and M. Overmars, *Computational Geometry — Algorithms and Applications*, Springer-Verlag, New York, 2008.